Chinese Chemical Letters 33 (2022) 2065–2068

Contents lists available at ScienceDirect

Chinese Chemical Letters

journal homepage: www.elsevier.com/locate/cclet

Enhancing photocatalytic performance of metal-organic frameworks for CO_2 reduction by a bimetallic strategy

Jihong Zhang[1], Yuchen Wang[1], Hongjuan Wang*, Dichang Zhong*, Tongbu Lu

MOE International Joint Laboratory of Materials Microstructure, Institute for New Energy Materials and Low Carbon Technologies, School of Materials Science and Engineering, Tianjin University of Technology, Tianjin 300384, China

ARTICLE INFO

Article history:
Received 10 July 2021
Revised 19 August 2021
Accepted 7 September 2021
Available online 13 September 2021

Keywords:
Metal-organic framework
Photocatalytic CO_2 reduction
Bimetallic strategy
CO_2–to–CO conversion
Photocatalysis
Dinuclear metal synergistic catalysis

ABSTRACT

Metal-organic frameworks (MOFs) as a type of crystalline heterogeneous catalysts have shown potential application in photocatalytic CO_2 reduction. However, MOF catalysts with high efficiency and selectivity are still in pursuit. Herein, by a bimetallic strategy, the catalytic performance of a Co-MOF for photocatalytic CO_2 reduction was enhanced. Specifically, the Co-MOF based on 4,5-dicarboxylic acid (H_3IDC) and 4,4′-bipydine (4,4′-bpy) can catalyze CO_2 reduction to CO, with high efficiency but relatively low selectivity. After replacement of 2/3 Co(II) with Ni(II) within Co-MOF, the resulted isostructural Co_1Ni_2-MOF not only retains high efficiency for photocatalytic CO_2 reduction, but also shows enhanced CO selectivity. The CO evolution rate reaches 1160 μmol g^{-1} h^{-1} and the CO selectivity reaches as high as 94.6%. The enhanced photocatalytic CO_2 reduction performance is supported by theoretical calculation results. This case demonstrates that bimetallic strategy is an effective mean to optimize the catalytic performance of MOF catalysts for photochemical CO_2 reduction.

Converting atmospheric excessive carbon dioxide (CO_2) into fuel or useful chemicals driven by sunlight is a sustainable approach to relieve energy shortage and environment deterioration [1–9]. The key is the development of efficient, selective and cheap catalysts. Metal-organic frameworks (MOFs) are a class of crystalline porous materials composed of metal ions (or metal clusters) and organic linkers [10–18]. With structural diversity and ultrahigh surface area, MOFs can serve as promising photocatalysts for CO_2 conversion, especially for those constructed from transition metals [19–23]. For instance, Wang group reported that Co-ZIF-9 can photocatalyze CO_2 reduction to CO, with the yield rate of 83.6 μmol/h and a selectivity of 58% [24]. Lan and co-workers developed a stable Co(II) MOF for CO_2 reduction [25], which showed a CO evolution rate of 1140 μmol g^{-1} h^{-1} and a selectivity of 47.4%. Obviously, although great progress in developing MOFs-based photocatalysts for photocatalytic CO_2 reduction has been achieved, the activity and selectivity of these catalysts still need to be further enhanced [26–33]. Very recently, we and others have demonstrated that the catalytic performance of metal complexes for photochemical CO_2 reduction can be improved by changing the metal centers and ligand modification [34–36]. We have also found that the dinuclear metal synergistic catalysis (DMSC) within dinuclear metal complexes can greatly boost the photocatalytic CO_2 reduction activity [37–39].

To further improve the catalytic performance of molecule-based materials for photochemical CO_2 reduction, we tried to build heterogeneous catalysts with DMSC. Herein, we report a case well demonstrating a bimetallic strategy for greatly increase the photocatalytic CO_2 reduction performance. Specifically, a Co-MOF based on mixed ligands of 4,5-dicarboxylic acid (H_3IDC) and 4,4′-bipydine (4,4′-bpy) [40] can efficiently catalyze CO_2 reduction to CO, while the selectivity to CO is relatively low. By gradually replacing the Co(II) with Ni(II) within Co-MOF, the CO selectivity of the resulted isostructural Co_xNi_y-MOFs (x and y represent the atomic ratio of Co and Ni, respectively) remarkably increases. The optimized Co_1Ni_2-MOF catalyst shows the best photocatalytic performance for CO_2 reduction, with a CO evolution rate of 1160 μmol g^{-1} h^{-1} and a selectivity of 94.6%. This work will pave a new way for developing high-performance MOFs-based catalysts for photocatalytic CO_2 reduction.

The Co-MOF was synthesized according to the reported procedure by Cao group [40]. The synthetic procedure of Ni-MOF was similar to that of Co-MOF (see Supporting information). Single-crystal X-ray diffraction indicated that Ni-MOF is isostructural with Co-MOF (Tables S1–S3 in Supporting information), where the Ni(II)

* Corresponding authors.
E-mail addresses: hongjuanwang@tjut.edu.cn (H. Wang), dczhong@email.tjut.edu.cn (D. Zhong).
[1] These authors contributed equally to this work.

https://doi.org/10.1016/j.cclet.2021.09.035
1001-8417/

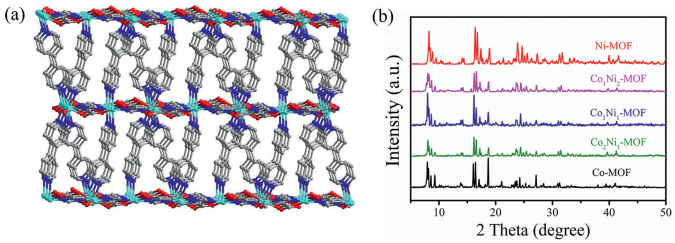

Fig. 1. (a) Three-dimensional pillar-layered structure of Co_xNi_y-MOFs; (b) PXRD patterns of Co_xNi_y-MOFs.

are linked with H_3IDC to form a two-dimensional (2D) layers with hexagonal 24-membered rings, and the 4,4′-bpy ligands pillar these layers to yield a three-dimensional (3D) pillar-layered framework (Fig. 1a). The powder X-ray diffraction (XRD) patterns of the as-synthesized Co-MOF and Ni-MOF agree well with the simulated ones (Fig. S1 in Supporting information), demonstrating the successful syntheses of both MOFs. Simultaneously, a series of isomorphic bimetallic Co_xNi_y-MOFs were tried to be synthesized by adding a certain amount of Ni(II) to the Co-MOF synthetic system. A remarkable color change of the bimetallic Co_xNi_y-MOFs, from orange to yellow green were observed with the gradual replacement of the Co(II) with Ni(II) (Fig. S2 in Supporting information). The similar cuboids morphology and powder XRD patterns (Fig. 1b and Fig. S3 in Supporting information) indicate that the synthesized bimetallic Co_xNi_y-MOFs maintained similar structures to that of monometallic MOF. The similar fourier transform infrared spectrometer (FT-IR) spectra and thermogravimetric (TG) curves further prove that these MOFs are isostructural (Figs. S4 and S5 in Supporting information). The CO_2 sorption experiments demonstrated that they also exhibit similar CO_2 uptake capacity (Fig. S6 in Supporting information). The element mappings of Co_xNi_y-MOFs show that C, N, O, Co and Ni are uniformly distributed (Fig. S7 in Supporting information), and the inductively coupled plasma mass spectrometry (ICP-MS) further demonstrate that the Co/Ni atomic ratio in Co_xNi_y-MOFs is consistent with the Co/Ni ratio used in synthesis (Table S4 and Fig. S8 in Supporting information).

Photocatalytic CO_2 reduction experiments were performed at room temperature with Co_xNi_y-MOFs as catalysts, $[Ru(phen)_3](PF_6)_2$ as a photosensitizer, and triethanolamine (TEOA) as an electron donor in a mixture of 5 mL CO_2-saturated CH_3CN/H_2O (v/v = 4:1), irradiated by a 300 W Xe lamp with wavelengths over 420 nm (see Supporting information). The gaseous products were detected by gas chromatography, and the liquid products were examined by ion chromatography. As shown in Fig. 2a and Tables S5 and S6 (Supporting information), the monometallic Co-MOF exhibits good activity for CO_2 reduction, with a CO generation rate of 1247 μmol g^{-1} h^{-1} and a CO selectivity of 85.8%. Ni-MOF also displays catalytic activity for photochemical CO_2 reduction, with the CO generation rate of 597 μmol g^{-1} h^{-1} and almost 100% CO selectivity. Impressively, the bimetallic Co_xNi_y-MOFs show enhanced catalytic performance with the increase of the Ni content. Particularly for the CO selectivity, when the Co/Ni ratio is 1/2 (Co_1Ni_2-MOF), a high CO selectivity of 94.6% is achieved, higher than pure Co-MOF (85.8%). The CO evolution rate reaches as high as 1160 μmol g^{-1} h^{-1}, twice than that of Ni-MOF (Fig. 2b and Tables S5 and S6), and comparable to most reported MOFs-based catalysts (Table S7 in Supporting information). No liquid product was detected by ion chromatography (Fig. S9 in Supporting information). The results demonstrated herein clearly illustrate that bimetallic strategy is effective to build high-performance MOF catalysts for photochemical CO_2 reduction.

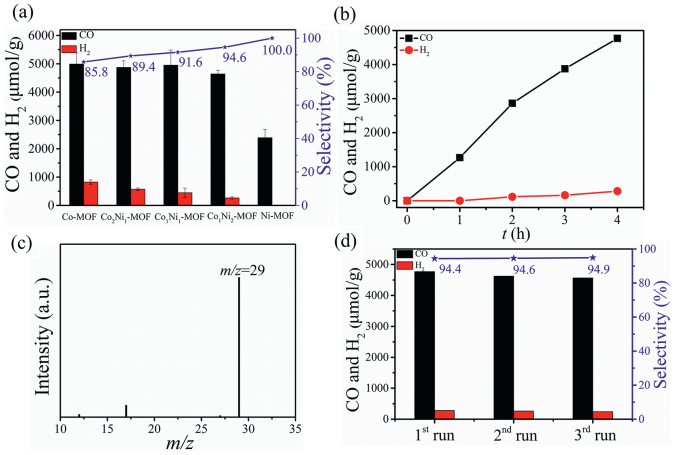

Fig. 2. (a) Photocatalytic CO_2 reduction with Co_xNi_y-MOFs; (b) Time profile of CO and H_2 evolution rate, (c) Mass spectrum of the gas generated from photocatalytic CO_2 reduction by using $^{13}CO_2$, (d) Cycle experiments of Co_1Ni_2-MOF for photocatalytic CO_2 reduction. Reaction conditions: catalyst (2 mg), $[Ru(phen)_3](PF_6)_2$ (0.43 mmol/L), TEOA (0.3 mol/L), CH_3CN/H_2O (v/v = 4:1; 5 mL), 300 W Xe lamp (λ > 420 nm), 4 h, 25 °C.

A series of control experiments with Co_1Ni_2-MOF were performed to identify the key factors for photochemical CO_2–to–CO conversion. As shown in Table S5, no product was detected in the absence of photosensitizer, TEOA or illumination, suggesting that the photosensitizer, sacrificial reductant, and light irradiation are all indispensable to CO_2–to–CO conversion (Table S5, entries 6–8 in Supporting information). In the absence of Co_1Ni_2-MOF, negligible CO was detected under the same condition (Table S5, Entry 9 in Supporting information). In addition, no CO was detected when Ar instead of CO_2 (Table S5, Entry 10 in Supporting information), illustrating that the CO was originated from the CO_2 reduction. Furthermore, in order to provide direct evidence for the carbon source of evolved CO, we performed an isotopic tracing experiment by replacing CO_2 with $^{13}CO_2$. As shown in Fig. 2c, the peak of m/z = 29 assigned to ^{13}CO was observed, solidly confirm that the produced CO originates from photocatalytic CO_2 reduction. To get the possibly higher catalytic activity of Co_1Ni_2-MOF, 12 mg of Co_1Ni_2-MOF was used for photocatalytic CO_2 reduction. The results show that the selectivity to CO also remains a high level of 94.7%, and 41.7 μmol CO was generated, much higher than that generated by 2 mg of Co_1Ni_2-MOF (9.3 μmol) under similar conditions. However, the CO yield rate did not increase accordingly (Fig. S10 in Supporting information). This may be ascribed to the small catalytic reactor, where many Co_1Ni_2-MOF could not fully contribute to the photocatalytic CO_2 reduction activity.

The photocatalytic stability is also crucial for catalysts. The cyclic catalytic experiments of Co_1Ni_2-MOF for photochemical CO_2 reduction show no noticeable activity decrease after three runs (Fig. 2d). The powder X-ray diffraction (PXRD) pattern, morphology and IR spectra of Co_1Ni_2-MOF after photocatalytic reaction are also similar to those freshly prepared. The above results illuminate that Co_1Ni_2-MOF is robust during photocatalytic CO_2 reduction process (Figs. S11–S13 in Supporting information). To reveal the catalytically active sites within Co_xNi_y-MOF, the photochemical CO_2 reduction experiments by Co_1Ni_2-MOF were carried out in the absence and presence of KSCN. The consistent PXRD pattern affirmed that the Co_1Ni_2-MOF maintain original crystal structure after treatment with KSCN (Fig. S14 in Supporting information). As Co_1Ni_2-MOF show dramatic activity decrease in the presence of KSCN, the Co/Ni in Co_1Ni_2-MOF can be assigned the catalytic centers for photocatalytic CO_2 reduction (Fig. S15 in Supporting information).

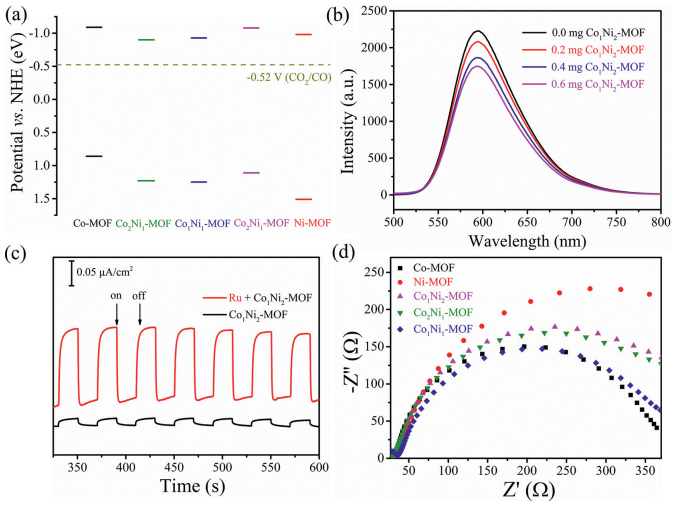

Fig. 3. (a) The band structures of Co_xNi_y-MOFs; (b) Steady state fluorescence spectra of $[Ru(phen)_3]PF_6$ upon the addition of Co_1Ni_2-MOF; (c) Photocurrent response of Co_1Ni_2-MOF and Co_1Ni_2-MOF containing $[Ru(phen)_3]PF_6$; (d) Nyquist plots of Co_xNi_y-MOFs.

To reveal the reason of increased catalytic performance of Co_1Ni_2-MOF, the optical properties and band gap energies of these materials were investigated by UV-vis diffuse reflectance spectroscopy (DRS, Fig. S16 in Supporting information). According to the Tauc plot, the corresponding band gaps were calculated to be 1.95 (Co-MOF), 2.13 (Co_2Ni_1-MOF), 2.18 (Co_1Ni_1-MOF), 2.19 (Co_1Ni_2-MOF) and 2.49 (Ni-MOF) eV *vs.* NHE (Figs. S17–S21 in Supporting information). By Mott Schottky plots (Figs. S22–S26 in Supporting information), the flat band position (V_{fb}) were determined to be −0.99 (Co-MOF), −0.8 (Co_2Ni_1-MOF), −0.83 (Co_1Ni_1-MOF), −0.98 (Co_1Ni_2-MOF) and −0.88 (Ni-MOF) eV *vs.* NHE, respectively. Since it is generally believed that the bottom of the conduction band (CB) in many n-type semiconductors is more negative by about 0.10 V than the V_{fb}, [41–45] the CB of Co-MOF, Co_2Ni_1-MOF, Co_1Ni_1-MOF, Co_1Ni_2-MOF and Ni-MOF was estimated to be −1.09, −0.9, −0.93, −1.08 and −0.98 eV, respectively. Combined with the results of band gaps, the valence band (VB) of Co_xNi_y-MOFs were estimated to be 0.86 (Co-MOF), 1.23 (Co_2Ni_1-MOF), 1.25 (Co_1Ni_1-MOF), 1.11 (Co_1Ni_2-MOF) and 1.51 (Ni-MOF) eV *vs.* NHE. Based on the above results, the energy-band alignment of Co-MOF, Co_xNi_y-MOFs and Ni-MOF can be drawn in Fig. 3a. Obviously, the CB potentials of Co_xNi_y-MOFs are more negative than the redox potential of photocatalytic CO_2 reduction to CO (−0.52 V *vs.* NHE), indicating that Co_xNi_y-MOFs satisfy the thermodynamic requirement of CO_2–CO conversion. In addition, the electrochemical experiments of Co_xNi_y-MOFs measured in 0.5 mol/L Na_2SO_4 under Ar/CO_2 showed larger current in CO_2 than in Ar, further indicating that Co_xNi_y-MOFs are potential catalysts capable of catalyzing CO_2 reduction (Figs. S27–S31 in Supporting information). The enhanced photocatalytic CO_2 reduction performance of Co_xNi_y-MOFs over Co-MOF/Ni-MOF also highlights the advantage of dimetallic catalysts. Compared with monometallic catalysts, the introduction of the second metal will change the interficial electronic structure and charge dispersion, which thus affects the photocatalytic performance.

In order to reveal the catalytic CO_2 reduction mechanism, room temperature photoluminescent (PL) quenching experiments of $[Ru(phen)_3](PF_6)_2$ were performed by addition of Co_1Ni_2-MOF or TEOA in a CO_2 degassed CH_3CN/H_2O solution (v/v = 4:1). As shown in Fig. 3b, the PL intensity of excited $[Ru(phen)_3]^{2+*}$ gradually decreases with the increase of the amount of Co_1Ni_2-MOF, which should be attributed to the electron transfer from

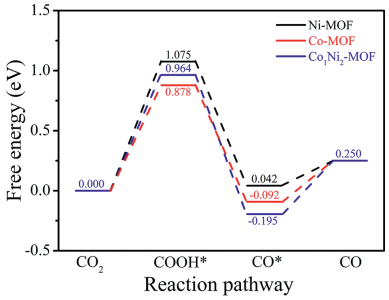

Fig. 4. Calculated free-energy diagrams for the conversion of CO_2 to CO.

the excited $[Ru(phen)_3]^{2+*}$ to Co_1Ni_2-MOF. By contrast, no obvious fluorescence decrease was observed with the addition of TEOA (Fig. S32 in Supporting information). Therefore, the quenched mode of the excited $[Ru(phen)_3]^{2+*}$ can be assigned to an oxidatively quenched pathway [46]. Photocurrent response measurements performed in several on–off cycles at a bias of −0.2 V *versus* Ag/AgCl showed that the Co_1Ni_2-MOF exhibits a small photocurrent response, while the photocurrent was greatly enhanced after addition of $[Ru(phen)_3](PF_6)_2$ (Fig. 3c). This observation indicates the rapid migration of photogenerated electrons of excited $[Ru(phen)_3]^{2+*}$ to Co_1Ni_2-MOF [41], which is consistent with the results of steady-state PL. In addition, electrochemical impedance spectroscopy (EIS) measurements showed that Co-MOF possesses a smallest capacitive loop diameter, Ni-MOF has a biggest one, and Co_xNi_y-MOFs are between those of Co-MOF and Ni-MOF (Fig. 3d). These results indicate that Ni-MOF has the largest charge-transfer resistance, which is consistent with the relatively lower catalytic activity of Ni-MOF.

Based on the above discussion, the photocatalytic mechanism of Co_xNi_y-MOFs for CO_2 reduction was proposed. Upon visible-light irradiation, the photosensitizer $[Ru(phen)_3]^{2+}$ is excited to form $[Ru(phen)_3]^{2+*}$, which is immediately quenched by Co_1Ni_2-MOF to generate the oxidized $[Ru(phen)_3]^{3+}$. Meanwhile, the excited electrons are transferred to CO_2 molecules adsorbed in Co_1Ni_2-MOF, leading to the activation and reduction of CO_2. The oxidized $[Ru(phen)_3]^{3+}$ is reduced to $[Ru(phen)_3]^{2+}$ by TEOA, to complete the entire catalytic cycle.

DFT calculations were further performed to understand the catalytic performance of Ni-MOF, Co_1Ni_2-MOF and Co-MOF for the conversion of CO_2 to CO (Fig. S33 in Supporting Information). The proposed reaction pathways and the corresponding free-energy diagrams are shown in Fig. 4. First, the CO_2 molecule undergoes a proton coupled electron transfer (PCET) process to form the COOH* intermediate (asterisk denotes an adsorption status), which is generally regarded as the rate-limiting step. The free energy change (ΔG) for this step over Ni-MOF, Co_1Ni_2-MOF and Co-MOF is 1.075, 0.964 and 0.878 eV, respectively. The results demonstrate that Co-MOF and Co_1Ni_2-MOF have appropriate ΔG values in the rate-limiting step, while Ni-MOF exhibits a relatively higher ΔG value. Then, the COOH* intermediate undergoes the second PCET process, forming *CO and a H_2O molecule. The ΔG values for this step over the three catalysts are negative (–1.033, –1.159 and –0.970 eV, respectively), indicating this step is spontaneous. Finally, the CO desorbs from the catalyst surface. For Ni-MOF, Co_1Ni_2-MOF, and Co-MOF, the CO desorption is slightly endothermic (0.208, 0.445 and 0.342 eV, respectively). Overall, the DFT calculations show that Co-MOF and Co_1Ni_2-MOF have better catalytic capacity for CO_2 to CO conversion than Ni-MOF, which well supports the experimental results.

In summary, a series of isostructural Co_xNi_y-MOFs based on H_3IDC and 4,4′-bpy were synthesized for photocatalytic CO_2 reduction. The experimental and DFT calculation results reveal

that bimetallic strategy is an effective way to optimize the photocatalytic performance of Co-MOF. The optimized bimetallic Co_1Ni_2-MOF exhibits remarkably enhanced photocatalytic performance for CO_2–to–CO conversion, with an evolution rate of 1160 μmol g^{-1} h^{-1} and a high selectivity of 94.6%, superior to those of monometallic Ni-MOF and Co-MOF. This work paves a new way for developing high-performance MOFs-based catalysts for photochemical CO_2 reduction.

Declaration of competing interest

We declare that we have no competing interests for the manuscript entitled “Enhancing photocatalytic performance of metal-organic frameworks for CO_2 reduction by bimetallic strategy”.

Acknowledgments

This work was financially supported by the National Key R&D Program of China (No. 2017YFA0700104), the National Natural Science Foundation of China (Nos. 22071182, 21861001, 21931007 and 21790052), the 111 Project of China (No. D17003) and the Science & Technology Development Fund of Tianjin Education Commission for Higher Education (No. 2018KJ129).

Supplementary materials

Supplementary material associated with this article can be found, in the online version, at doi:10.1016/j.cclet.2021.09.035.

References

[1] M. Mikkelsen, M. Jørgensen, F.C. Krebs, Energy Environ. Sci. 3 (2010) 43–81.
[2] J. Artz, T.E. Muller, K. Thenert, Chem. Rev. 118 (2018) 434–504.
[3] D.C. Liu, D.C. Zhong, T.B. Lu, Energy Chem. 2 (2020) 100034.
[4] D. Kim, K.K. Sakimoto, D.C. Hong, P.D. Yang, Angew. Chem. Int. Ed. 54 (2015) 3259–3266.
[5] C.A. Deutsch, J.J. Tewksbury, M. Tigchelaar, et al., Science 361 (2018) 916–919.
[6] J.W. Liu, C.Y. Chen, K. Zhang, L. Zhang, Chin. Chem. Lett. 32 (2021) 649–659.
[7] P.V. Kamat, Acc. Chem. Res. 50 (2017) 527–531.
[8] W. Yang, J.H. Zhang, R. Si, et al., Inorg. Chem. Front. 8 (2021) 1695–1701.
[9] J.L. White, M.F. Baruch, Y. Hu, et al., Chem. Rev. 115 (2015) 12888–12935.
[10] Y.H. Luo, L.Z. Dong, J. Liu, S.L. Li, Y.Q. Lan, Coord. Chem. Rev. 390 (2019) 86–126.
[11] J.H. Deng, Y.Q. Wen, J. Willman, et al., Inorg. Chem. 58 (2020) 11020–11027.
[12] J. Meng, X. Liu, C.J. Niu, et al., Chem. Soc. Rev. 49 (2020) 3142–3186.
[13] Y.N. Gong, J.H. Mei, J.W. Liu, et al., Appl. Catal. B: Environ. 292 (2021) 120156.
[14] W.G. Lu, Z.W. Wei, Z.Y. Gu, et al., Chem. Soc. Rev. 43 (2014) 5561–5593.
[15] J.H. Zhang, W. Yang, M. Zhang, et al., Nano Energy 80 (2021) 105542.
[16] X.Z. Fang, Q.C Shang, Y. Wang, et al., Adv. Mater. 30 (2018) 1705112.
[17] X.B. Liu, T. Yue, K. Qi, et al., Chin. Chem. Lett. 31 (2020) 2189–2201.
[18] Y. Wang, S.B. Wang, X.W. Lou, Angew. Chem. Int. Ed. 58 (2019) 17236–17240.
[19] M. Ding, R.W. Flaig, H.L. Jiang, O.M. Yaghi, Chem. Soc. Rev. 48 (2019) 2783–2828.
[20] F.H. Mu, B.L. Dai, W. Zhao, et al., Chin. Chem. Lett. 31 (2020) 1773–1781.
[21] Y. Wang, N.Y. Huang, J.Q. Shen, et al., J. Am. Chem. Soc. 140 (2018) 38–41.
[22] W. Yang, H.J. Wang, R.R. Liu, et al., Angew. Chem. Int. Ed. 60 (2021) 409–414.
[23] G. Wang, C.T. He, R. Huang, et al., J. Am. Chem. Soc. 142 (2020) 19339–19345.
[24] S.B. Wang, Yao W.S, J.L. Lin, Z.X. Ding, X.C. Wang, Angew. Chem. Int. Ed. 53 (2014) 1034–1038.
[25] X.K. Wang, J. Liu, L. Zhang, et al., ACS Catal. 9 (2019) 1726–1732.
[26] J.W. Liu, L.F. Chen, H. Cui, et al., Chem. Soc. Rev. 43 (2014) 6011–6061.
[27] B. An, Z. Li, Y. Song, et al., Nat. Catal. 2 (2019) 709–717.
[28] Z. Jiang, X.H. Xu, Y.H. Ma, et al., Nature 586 (2020) 549–554.
[29] L.Z. Dong, L. Zhang, J. Liu, et al., Angew. Chem. Int. Ed. 59 (2020) 2659–2663.
[30] H.Q. Zhang, H.T. Xu, Y.Y. Li, X.B. Pan, L.S. Li, Sci. China Mater. 63 (2020) 769–778.
[31] Y. Wang, S.B. Wang, S.L. Zhang, X.W. Lou, Angew. Chem. Int. Ed. 59 (2020) 11918–11922.
[32] S.B. Wang, B.Y. Guan, X.W. Lou, Energy Environ. Sci. 11 (2018) 306–310.
[33] P.P. Niu, Z.M. Pan, S.B. Wang, X.C. Wang, ChemSusChem 14 (2021) 1302–1307.
[34] D.C. Liu, H.H. Huang, J.W. Wang, et al., ChemCatChem 10 (2018) 3435–3440.
[35] D.C. Liu, H.J. Wang, T. Ouyang, et al., ACS Appl. Energy Mater. 1 (2018) 2452–2459.
[36] D.C. Liu, H.J. Wang, J.W. Wang, et al., Chem. Commun. 54 (2018) 11308–11311.
[37] T. Ouyang, H.H. Huang, J.W. Wang, D.C Zhong, T.B. Lu, Angew. Chem. Int. Ed. 56 (2017) 738–743.
[38] L.M. Cao, H.H. Huang, J.W. Wang, D.C Zhong, T.B. Lu, Green Chem. 20 (2018) 798–803.
[39] T. Ouyang, H.J. Wang, H.H. Huang, et al., Angew. Chem. Int. Ed. 57 (2018) 16480–16485.
[40] Y.L. Wang, D.Q. Yuan, W.H. Bi, et al., Cryst. Growth Des. 5 (2005) 1849–1855.
[41] H. Dong, X. Zhang, Y. Lu, et al., Appl. Catal. B: Environ. 276 (2020) 119173.
[42] F.M. Zhang, J.L. Sheng, Z.D. Yang, et al., Angew. Chem. Int. Ed. 57 (2018) 12106–12110.
[43] J. Zhang, X. Chen, K. Takanabe, et al., Angew. Chem. Int. Ed. 122 (2010) 451–454.
[44] A. Ishikawa, T. Takata, J.N. Kondo, et al., J. Am. Chem. Soc. 124 (2002) 13547–13553.
[45] Y. Matsumoto, J. Solid State Chem. 126 (1996) 227–234.
[46] H.X. Zhang, Q.L. Hong, J. Li, et al., Angew. Chem. Int. Ed. 58 (2019) 11752–11756.